ESC European Society of Cardiology

European Heart Journal (2018) **39**, 1602–1609
doi:10.1093/eurheartj/ehx810

CLINICAL RESEARCH
Interventional cardiology

Endothelial shear stress 5 years after implantation of a coronary bioresorbable scaffold

Vikas Thondapu[1,2†], Erhan Tenekecioglu[3†], Eric K.W. Poon[1], Carlos Collet[4,5], Ryo Torii[6], Christos V. Bourantas[7,8], Cheng Chin[9], Yohei Sotomi[4], Hans Jonker[10], Jouke Dijkstra[11], Eve Revalor[2,12], Frank Gijsen[13], Yoshinobu Onuma[3], Andrew Ooi[1], Peter Barlis[2], and Patrick W. Serruys[3,14]*

[1]Department of Mechanical Engineering, Melbourne School of Engineering, University of Melbourne, Parkville, 3010 Victoria, Australia; [2]Department of Medicine, Faculty of Medicine, Dentistry & Health Sciences, Melbourne Medical School, University of Melbourne, Parkville, 3010 Victoria, Australia; [3]Department of Interventional Cardiology, Erasmus University Medical Centre, Thoraxcenter, Westblaak 98, 3012 KM Rotterdam, Netherlands; [4]Department of Cardiology, Academic Medical Center, University of Amsterdam, Meibergdreef 9, 1105 AZ Amsterdam-Zuidoost, The Netherlands; [5]Department of Cardiology, University Hospital Brussels, Avenue du Laerbeek 101, 1090 Jette, Belgium; [6]Department of Mechanical Engineering, University College London, Torrington Place, WC1E 7JE London, UK; [7]Department of Cardiology, Barts Heart Centre, Barts Health NHS Trust, West Smithfield, EC1A 7BE London, UK; [8]Institute of Cardiovascular Sciences, University College London, 62 Huntley St, Fitzrovia, WC1E 6DD London, UK; [9]School of Mechanical Engineering, The University of Adelaide, Adelaide, 5005 South Australia, Australia; [10]Department of Program Management, Cardialysis, Westblaak 98, 3012 KM Rotterdam, The Netherlands; [11]Department of Radiology, Leiden University Medical Center, Albinusdreef 2, 2333 ZA, Leiden, The Netherlands; [12]Department of Biomedical Engineering, Melbourne School of Engineering, University of Melbourne, 3010 Parkville, Australia; [13]Department of Biomedical Engineering, Thoraxcenter, Erasmus University Medical Center, Wytemaweg 80, Ee2302, 3015 CN Rotterdam, The Netherlands; and [14]Cardiovascular Science Division, National Heart & Lung Institute, Guy Scadding Building, Royal Brompton Campus, Imperial College, London, UK

Received 18 July 2017; revised 26 October 2017; editorial decision 21 December 2017; accepted 9 January 2018; online publish-ahead-of-print 2 February 2018

Aims As a *sine qua non* for arterial wall physiology, local hemodynamic forces such as endothelial shear stress (ESS) may influence long-term vessel changes as bioabsorbable scaffolds dissolve. The aim of this study was to perform serial computational fluid dynamic (CFD) simulations to examine immediate and long-term haemodynamic and vascular changes following bioresorbable scaffold placement.

Methods and results Coronary arterial models with long-term serial assessment (baseline and 5 years) were reconstructed through fusion of intravascular optical coherence tomography and angiography. Pulsatile non-Newtonian CFD simulations were performed to calculate the ESS and relative blood viscosity. Time-averaged, systolic, and diastolic results were compared between follow-ups. Seven patients (seven lesions) were included in this analysis. A marked heterogeneity in ESS and localised regions of high blood viscosity were observed post-implantation. Percent vessel area exposed to low averaged ESS (<1 Pa) significantly decreased over 5 years (15.92% vs. 4.99%, $P < 0.0001$) whereas moderate (1–7 Pa) and high ESS (>7 Pa) did not significantly change (moderate ESS: 76.93% vs. 80.7%, $P = 0.546$; high ESS: 7.15% vs. 14.31%, $P = 0.281$), leading to higher ESS at follow-up. A positive correlation was observed between baseline ESS and change in lumen area at 5 years ($P < 0.0001$). Maximum blood viscosity significantly decreased over 5 years (4.30 ± 1.54 vs. 3.21 ± 0.57, $P = 0.028$).

Conclusion Immediately after scaffold implantation, coronary arteries demonstrate an alternans of extremely low and high ESS values and localized areas of high blood viscosity. These initial local haemodynamic disturbances may trigger fibrin deposition and thrombosis. Also, low ESS can promote neointimal hyperplasia, but may also contribute to appropriate scaffold healing with normalisation of ESS and reduction in peak blood viscosity by 5 years.

Keywords Bioabsorbable scaffold • Shear stress • Blood viscosity

* Corresponding author. Tel: +31 010 206 2828, Fax: +31 010 206 2844, Email: patrick.w.j.c.serruys@pwserruys.com

† The first two authors contributed as co-first author.

Introduction

The fundamental concept of a stent and its complications has not changed greatly since pioneering work in the early 20th century.[1] The technology underlying these devices, however, has undergone great and rapid advances that seem, perhaps, to be accelerating.

Despite excellent clinical outcomes with current generation of metallic drug-eluting stents, their permanent nature remains a theoretical limitation. In that sense, the adoption of bioresorbable materials is one recent leap forward in stent technology. The ideal bioresorbable stent is meant to fulfil a temporary function as a vascular scaffold to aid vessel healing and stabilisation, and then disappear.

The Absorb Bioresorbable Vascular Scaffold (BVS, Abbott Vascular, Santa Clara, CA, USA) has been the most implanted and studied bioresorbable scaffold. The longest-term clinical data currently available indicates 5-year outcomes similar to standard comparator metallic drug-eluting stents.[2,3] Resorption of the Absorb may also be accompanied by a partial and gradual return of normal vasomotion, late lumen enlargement, and plaque stabilisation.[4–8] However, recent evidence from larger trials shows that while rare, late thrombosis occurs more frequently with the Absorb scaffold.[9–11] There remain many unanswered questions regarding the mechanisms of late scaffold complications, but certain clues may lie in the dynamics of blood flow after scaffolding.

Fluid shear stress exerted by blood flow directly regulates vascular physiology and pathology.[12,13] Changes in arterial geometry induced by stent or scaffold placement can significantly change blood flow throughout the vessel,[14,15] thereby altering the macro-level shear stress distribution. Individual stent struts may themselves disturb flow at an even smaller scale near the endothelium,[16–19] creating so-called micro-level disturbances. After implantation, such macro- and micro-level flow disturbances may have repercussions not only for the development of scaffold thrombosis and restenosis, but also for appropriate neointimal healing and vessel remodelling.

The aim of this study was to perform serial high-fidelity computational fluid dynamic (CFD) simulations to examine immediate and long-term haemodynamic and vascular changes following bioresorbable scaffold placement.

Methods

Patient selection and study design

Patients with serial imaging from the ABSORB Cohort B clinical trial were retrospectively identified for further computational analysis. The original study design and protocol have been previously described.[20] Patients underwent serial invasive imaging with coronary angiography and optical coherence tomography (OCT) immediately after scaffold implantation and again at 5 years.

Exclusion criteria were lack of two angiographic views separated by >25°, excessive vessel foreshortening, suboptimal OCT images, and side branches >2 mm within the scaffold which prohibited 3D reconstruction. Angiography and OCT images from each time point were fused to reconstruct 3D models of the scaffolded artery at baseline and 5 years. Computational fluid dynamic analysis was then performed to calculate endothelial shear stress (ESS) and local blood viscosity at baseline and 5 years.

Image acquisition and data analysis

Optical coherence tomography is an intravascular imaging technique providing high-resolution (10–20 μm) cross-sectional images of coronary arteries and scaffolds.[21] Optical coherence tomography was performed immediately after scaffold implantation and at 5 years in all treated coronary arteries using a frequency-domain OCT system (C7-XR or C8XR OCT Intravascular Imaging System; St. Jude Medical, St. Paul, MN, USA). All image acquisitions were performed using non-occlusive contrast flushing according to standard guidelines.[21] Angiography was performed as previously described.[20]

Three-dimensional arterial reconstruction

For each time point, OCT and angiography were fused to reconstruct patient-specific 3D models of the scaffolded artery at baseline and 5 years (*Figure 1*).[22] Briefly, dual plane end-diastolic angiographic images (orthogonal views >25° difference) were used to extract the 3D luminal centreline (QAngio XA 3D, Medis Specials Bv, Netherlands). The radiopaque scaffold markers and side branches were used as landmarks to co-register angiography with OCT. The OCT lumen and scaffold contours were semi-automatically detected (QCU-CMS v4.69, LKEB, Leiden University, Netherlands). The contours were placed onto the angiographic centreline using scaffold markers and vessel landmarks to correct the rotational and longitudinal orientation of the OCT frames (MATLAB R2015b, Mathworks Inc., Natick, MA, USA), and the baseline and 5-year scaffolded vessel surfaces were generated (Meshlab, Visual Computing Lab ISTI-CNR, Pisa, Italy).[23]

Computational fluid dynamic simulation

Each reconstruction was discretised into approximately 30 million tetrahedral elements using ICEM CFD v15.0 (ANSYS Inc., Canonsburg, PA, USA). Computational fluid dynamic analysis was accomplished through direct solution of the incompressible Navier–Stokes equations describing fluid motion (OpenFOAM-2.1.1, OpenCFD Ltd, ESI group, Bracknell, UK). A time-varying (pulsatile) parabolic velocity profile with a mean inlet flow of 1.3 cc/s was applied at the inlet. The arterial wall was considered rigid with a no-slip boundary and a non-specific distal vascular resistance was applied at the outlet. Blood density was assumed 1060 kg/m^3 and haematocrit 45%. Non-Newtonian blood behaviour was modelled using the Quemada equation, in which viscosity varies depending on shear rate and haematocrit.[24] OpenFOAM was run on the Victorian Life Sciences Computation Initiative (VLSCI) supercomputer consisting of 1024 IBM Blue Gene/Q CPUs at 1.6 GHz (IBM Research, Australia).

Endothelial shear stress was calculated as the product of viscosity and velocity gradient (shear rate) at the wall. For quantitative calculations ESS was classified as low (<1 Pa), moderate (1–7 Pa), or high (>7 Pa) (see Supplementary material online, Methods).[25–27] Percent lumen area exposed to low, moderate, and high ESS at systolic, diastolic, and time-averaged flow was determined at baseline and 5 years. In order to assess the change in lumen dimensions, the baseline and 5-year arterial reconstructions were matched by using the scaffold markers and anatomical landmarks. The impact of baseline ESS on the change in lumen area was investigated.

Due to its shear-thinning properties, blood exhibits higher viscosity at low shear rates and approaches a constant low viscosity at high shear rates. Computational fluid dynamic simulations using a Newtonian model of blood behaviour assume that shear rate is high enough that viscosity is constant (0.0035 Pa s). However, the non-Newtonian model used in this study allowed direct calculation of local blood viscosity,[24] which was expressed as a ratio of non-Newtonian to constant Newtonian viscosity[28,29] and henceforth referred to as relative viscosity. Maximum relative blood viscosity was determined at systolic, diastolic, and time-averaged flow at baseline and 5 years.

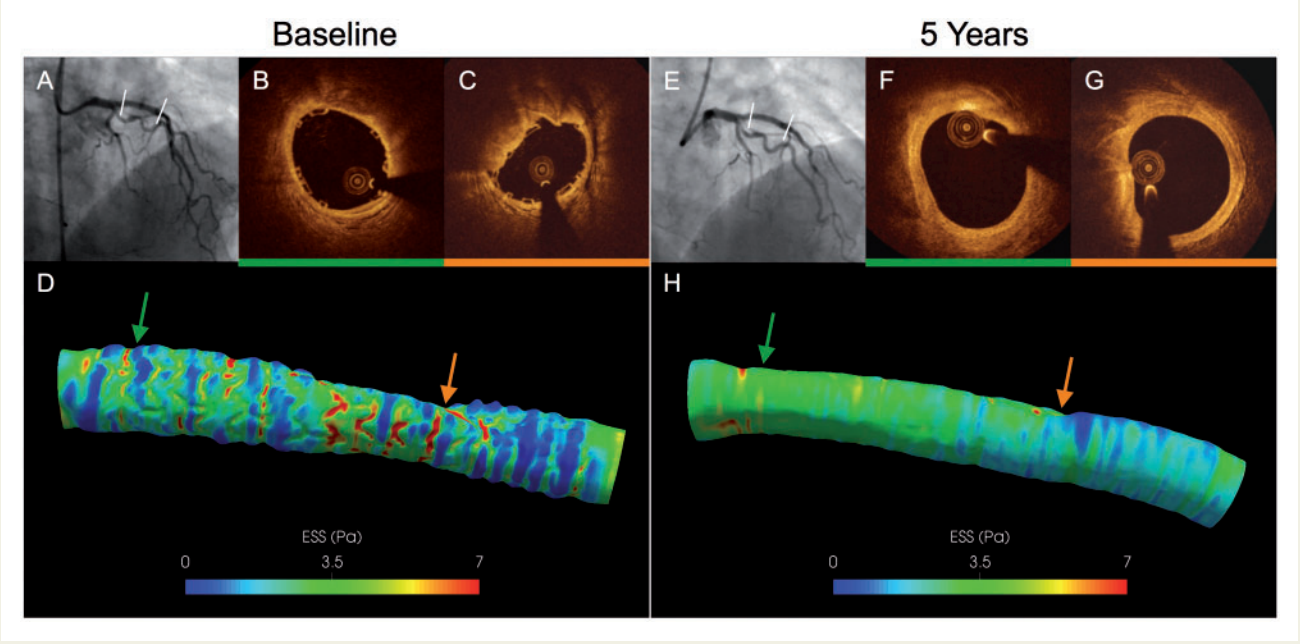

Figure 1 Three-dimensional arterial models were reconstructed from the fusion of angiography and optical coherence tomography. (*A*, *E*) Angiography was used to extract the vessel centreline in the scaffolded segment (between white lines). (*B*, *C*, *F*, *G*) Optical coherence tomography images were used to generate the detailed lumen and scaffold surface. Representative optical coherence tomography images show the same locations at baseline and 5 years (green and orange arrows). (*D*, *H*) Computational fluid dynamic simulations were performed to calculate endothelial shear stress and local blood viscosity. ESS, endothelial shear stress.

Statistical analysis

Continuous variables were reported as mean (standard deviation) if they followed a Gaussian distribution. Binary variables were reported as counts and percentages. Changes in ESS between baseline and 5 years were compared with a generalized linear mixed-effect model with a random intercept. To examine the association between baseline shear stress and changes in luminal area a one-level hierarchical linear model was used. No formal hypothesis testing was planned. A Wilcoxon rank sum test was used to evaluate the change in relative blood viscosity. All *P*-values were two-sided. However, the *P*-values presented are exploratory analyses only, and should therefore be interpreted cautiously. A non-parametric Robust method (CLSI C28-A3) was used to calculate 95% confidence interval.[30] Data analysis was performed using SPSS, version 24 (Chicago, IL, USA).

Results

Seven patients (seven lesions) fulfilled the study criteria and were included in the present analysis. The scaffold was implanted the left anterior descending coronary artery (5), left circumflex artery (1), and right coronary artery (1). Patient characteristics are demonstrated in *Table 1*. Procedural characteristics are shown in *Table 2*. None of the patients developed adverse clinical events including death, myocardial infarction, revascularisation, or scaffold thrombosis during 5 years of clinical observation (see Supplementary material online, *Table S1*).

Since peak coronary flow occurs during diastole, the vessel was exposed to predominantly high ESS (*Take home figure A* and *C*) without evidence of micro-recirculation. During systole, a rapid drop in coronary flow results in exposure to very low ESS (*Take home figure B* and *D*) and, due to the steep negative flow gradient, unmasks micro-recirculation of blood between scaffold struts at baseline (*Take home figure B1 and B2*). By 5 years, ESS has homogenised to

Table 1 Baseline characteristics of the studied population ($n = 7$, lesions = 7)

Age (years)	62 ± 9
Male	4 (57)
Hypertension	3 (43)
Hypercholesterolaemia	5 (71)
Diabetes mellitus	0 (0)
Current smoking	1 (14)
Prior percutaneous coronary intervention	2 (29)
Prior myocardial infarction	2 (29)
Stable angina	5 (71)
Unstable angina	1 (14)
Silent ischaemia	0 (0)
Treated vessel	
Left anterior descending artery	5 (71)
Left circumflex artery	1 (14)
Right coronary artery	1 (14)
Ramus intermedius	0 (0)

Values are mean ± standard deviation or *n* (%).

Table 2 Procedural characteristics

	n = 7, lesions = 7
ACC/AHA lesion class	
A	0 (0)
B1	5 (71)
B2	2 (29)
C	0 (0)
Pre-dilatation	7/7 (100)
Mean pre-dilatation pressure (atm)	11.77 ± 2.56
Diameter of scaffolds (mm)	3.00 ± 0.0
Expected scaffold diameter (mm)	3.26 ± 0.10
Total length of study devices (mm)	18.0 ± 0.0
Nominal scaffold area (mm^2)	7.07 ± 0.0
Expected scaffold area (mm^2)	8.37 ± 0.53
Mean deployment pressure (atm)	13.00 ± 3.01
Post-dilatation	4/7 (57)
Mean post-dilatation pressure (atm)	17.64 ± 5.28
Procedural complications	0/7 (0)
Clinical device success	7/7 (100)
Clinical procedure success	7/7 (100)

Values are mean ± standard deviation or *n* (%).
ACC, American College of Cardiology; AHA, American Heart Association.

more physiological values and systolic micro-recirculation has dissipated (*Take home figure D1 and D2*).

Quantitative measurements demonstrate that although ESS distribution varied considerably through the cardiac cycle, the mean percent lumen area exposed to ESS <1 Pa significantly decreased between baseline and 5 years during diastolic, systolic, and time-averaged conditions (diastole: 6.90 vs. 2.78%, $P = 0.008$; systole: 53.31 vs. 38.37%, $P = 0.042$; time-averaged: 15.92 vs. 4.99%, $P < 0.0001$) (*Table 3*). Although individual cases demonstrated slightly different patterns of increases in moderate and high ESS (*Figure 2*) (see Supplementary material online, *Table S2*), overall mean vessel exposure to moderate and high ESS did not significantly change over 5 years in diastolic, systolic, or time-averaged flow conditions (*Table 3*).

Figure 3 represents the relationship between post-implantation ESS and the change in lumen area over 5 years. A positive association was observed ($y = 0.32x–1.49$; $P < 0.0001$), indicating that higher baseline ESS values after scaffold implantation were correlated with an increase in lumen area. A serial point-by-point analysis was also performed to investigate the change in lumen radius, and demonstrated a similar qualitative relationship to baseline ESS (*Figure 4*).

High blood viscosity was apparent in two broadly distinctive regions: at the centre of the artery where shear rate is low but blood velocity is high, and at specific locations near the lumen surface where both shear rate and blood velocity are low. Notably, near-wall regions of high blood viscosity were observed in the vicinity of

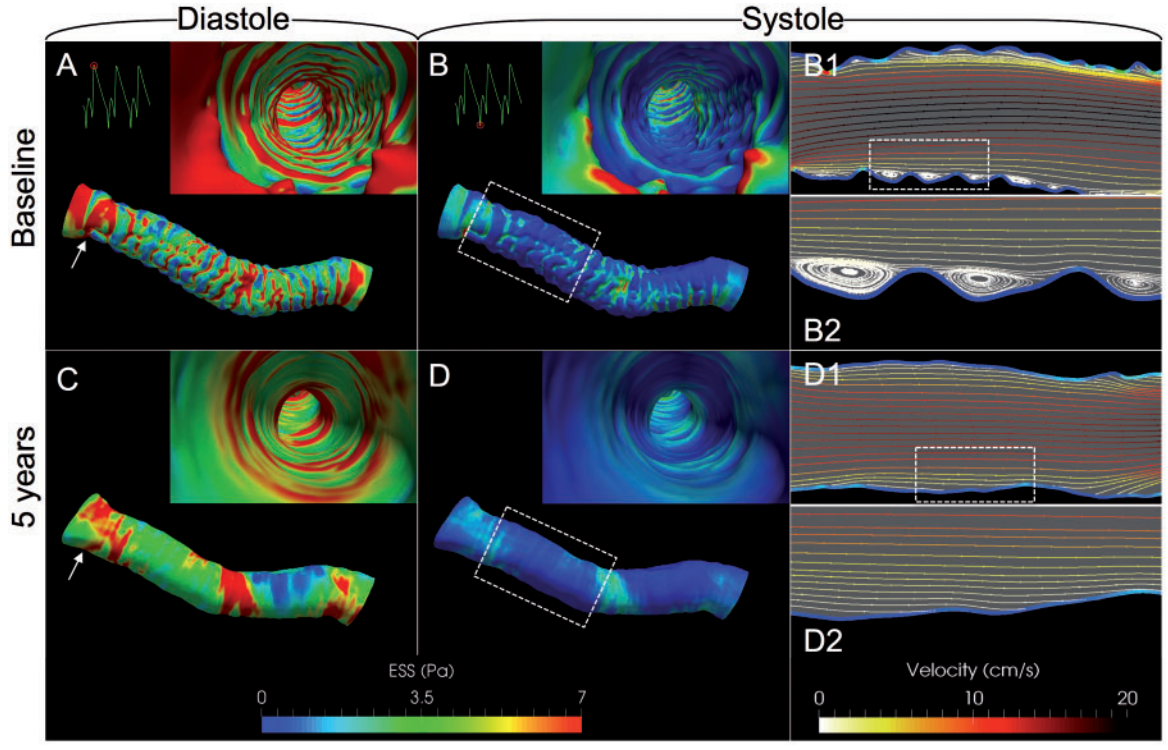

Take home figure Pulsatile computational fluid dynamic simulation provides detailed local haemodynamics in diastole and systole. (*A*, *B*) At baseline, the vessel has a corrugated appearance arising from high endothelial shear stress on top of scaffold struts and low endothelial shear stress in between. (*C*, *D*) At 5 years, only broad swaths of low, moderate, and high endothelial shear stress remain. (*B1*, *D1*) Cut-plane views of the area within the dashed white box in *B* and *D*, respectively, demonstrate laminar flow at the centre of the artery but micro-recirculation near the wall. By 5 years systolic micro-recirculation has been eliminated. (*B2*, *D2*) Enlarged view of area within the dashed white box in *B1* and *D1*, respectively, show that micro-recirculation occurs only at baseline between scaffold struts. ESS, endothelial shear stress.

Table 3 Pulsatility-dependent endothelial shear stress at baseline and 5 years, all cases combined

	Systole			Diastole			Time-averaged		
	Baseline (95% CI)	5 years (95% CI)	*P*-value	Baseline (95% CI)	5 years (95% CI)	*P*-value	Baseline (95% CI)	5 years (95% CI)	*P*-value
ESS <1	53.31 (14.23 to 102.61)	38.37 (-24.11 to 99.05)	0.042	6.9 (-5.02 to 17.74)	2.78 (-10.72 to 12.83)	0.008	15.92 (1.06 to 27.89)	4.99 (-10.42 to 18.16)	<0.0001
1< ESS <7	46.23 (-0.88 to 84.10)	58.98 (6.01 to 116.29)	0.067	68.79 (36.82 to 91.75)	61.28 (1.66 to 122.01)	0.434	76.93 (58.67 to 94.70)	80.7 (46.40 to 123.14)	0.546
ESS >7	0.46 (-1.65 to 2.03)	2.65 (0 to 9.89)	NS	24.31 (-6.06 to 58.17)	35.94 (-30.82 to 102.02)	0.218	7.15 (-8.16 to 20.21)	14.31 (-31.11 to 49.68)	0.281

Values are expressed as percent lumen area exposed to low, moderate, and high ESS.
CI, confidence interval; ESS, endothelial shear stress; NS, not significant.

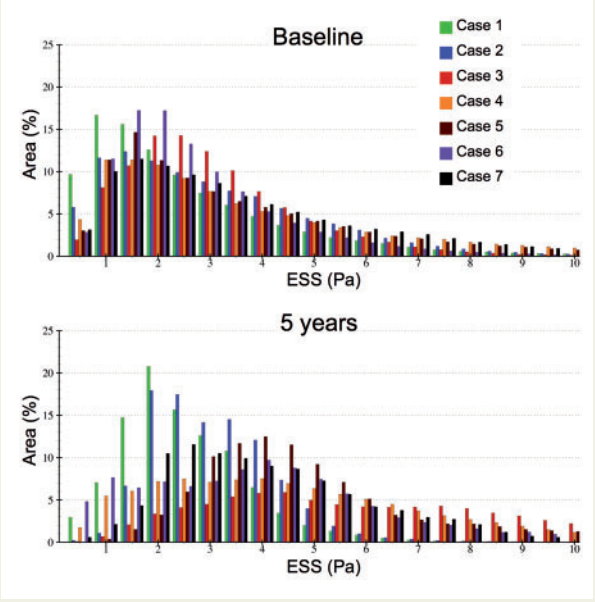

Figure 2 Histogram demonstrating percent of the lumen area exposed to various levels of endothelial shear stress at baseline and 5 years for each case. ESS, endothelial shear stress.

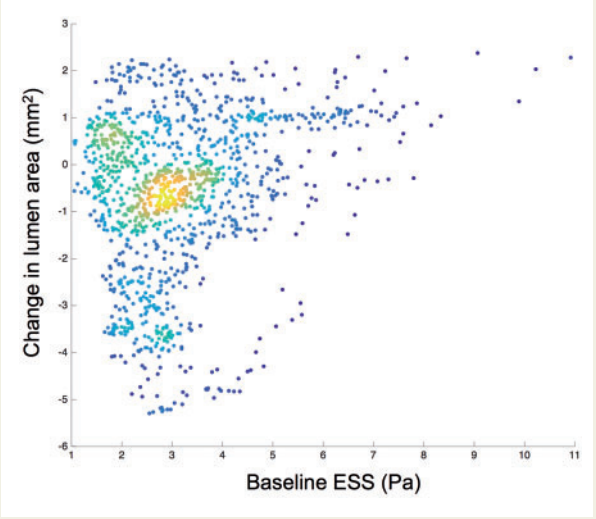

Figure 3 Scatterplot of baseline endothelial shear stress vs. the interval change in lumen area over 5 years for all cases combined, coloured by the relative density of data points (yellow indicates high density, blue indicates low density). Baseline and 5-year arterial reconstructions were precisely aligned and compared on a frame-by-frame basis. Higher baseline endothelial shear stress values are correlated with an increase in lumen area over 5 years. ESS, endothelial shear stress.

scaffold struts (*Figure 5*), corresponding to locations of micro-recirculation and low ESS.

Quantitative analysis of all seven cases demonstrated an approximately 35% higher time-averaged blood viscosity throughout the arteries than is conscribed by the Newtonian model. Although mean viscosity did not change, maximum relative viscosity significantly decreased over 5 years (systole: 8.84 vs. 5.33, $P = 0.043$; diastole: 4.46 vs. 3.18, $P = 0.063$; time-averaged: 4.30 vs. 3.21, $P = 0.028$) (*Table 4*). Like ESS, viscosity also fluctuated considerably throughout the cardiac cycle, peaking in systole for all cases at both baseline and 5 years (see Supplementary material online, *Table S3*). Remarkably, in Cases 1, 5, and 7 the maximum relative viscosity approached a 10-fold increase in some locations at baseline.

Discussion

The high fidelity CFD simulations conducted in this study revealed that haemodynamics in scaffolded coronary arteries are marked by wide fluctuation in ESS throughout the cardiac cycle, resulting in transient micro-recirculation, and pockets of high blood viscosity in the scaffolded region that largely disappear as the scaffold dissolves. This process was accompanied by vessel exposure to more physiological levels of ESS, reduced peak blood viscosity, and late lumen enlargement over 5 years.

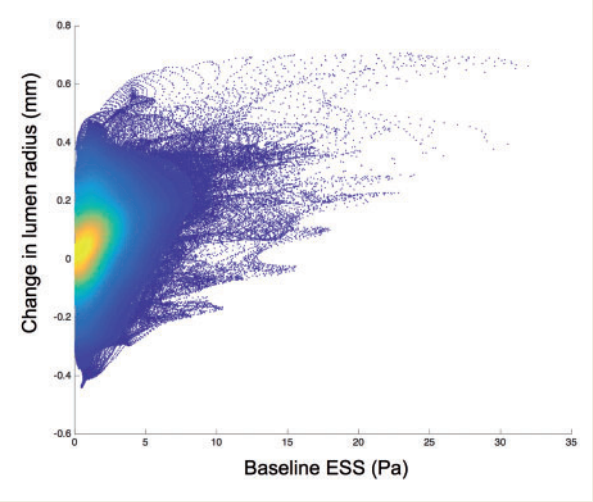

Figure 4 After optimal alignment, baseline and 5-year arterial reconstructions were compared on a point-by-point basis. A scatterplot of baseline endothelial shear stress vs. the interval change in lumen radius over 5 years from a single representative case, coloured by density of data points (yellow indicates high density; blue indicates low density). Qualitatively, higher baseline endothelial shear stress values are correlated with an increase in lumen radius at that point over 5 years. ESS, endothelial shear stress.

Bioresorbable medical devices have gained exceptional attention over recent years but there remain many unanswered questions about how these devices perform over time. These questions have been particularly relevant with the Absorb coronary scaffold, which has been hampered by late scaffold thrombosis.[2,10,11,31] The mechanisms are thought to involve late scaffold dismantling and inflammation,[8,32] but other factors governing scaffold outcomes could include local blood flow dynamics.

Fluid dynamic phenomena of blood flow directly regulate vascular biology and influence the development of atherosclerosis.[12,13] Abnormally low and high ESS have been correlated with atherosclerotic plaque progression, vulnerability, and perhaps even disruption, platelet activation, and subsequent thrombosis.[33–36] Similarly, changes in arterial geometry induced by stent or scaffold placement can also significantly alter blood flow and ESS distribution at the strut and vessel scale.[37] Such post-intervention flow disturbances may have repercussions for the development of scaffold thrombosis and restenosis.[15,18,38]

In order to gain new insights into local haemodynamics within scaffolded arteries, this study employed serial OCT imaging over 5 years as the basis for CFD analysis. Due to the use of pulsatile flow conditions and a non-Newtonian model of blood behaviour, these simulations are of unprecedented scope and detail. This methodology has allowed several key observations.

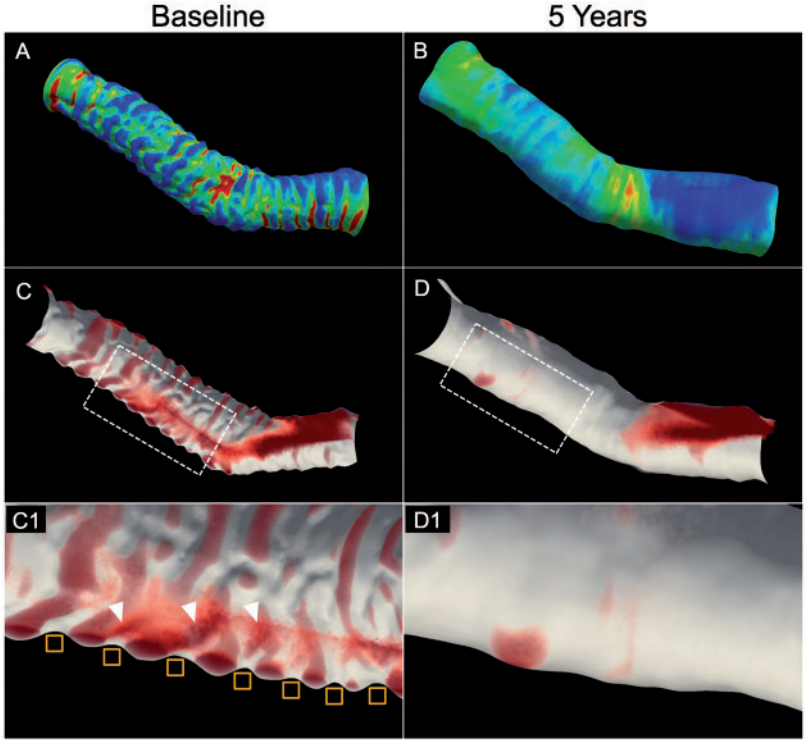

Figure 5 (*A*, *B*) Time-averaged endothelial shear stress within the scaffolded segment. (*C*, *D*) Longitudinal cut-plane view of the scaffolded segment, with volume-rendered near-wall regions of high blood viscosity. The lumen surface is solid white in colour. Regions of red indicate relative viscosity >1.4. (*C*) At baseline, regions of high viscosity localise to the inter-strut region and the distal segment of the curved artery. (*C1*) A closer view shows that after implantation, high viscosity may extend over struts and further into the lumen (white arrowheads). (*D*, *D1*) By 5 years, a region of high viscosity persists at the distal curvature, however, the inter-strut regions of high viscosity have largely disappeared.

Table 4 Local blood viscosity at baseline and 5 years, all cases combined

	Systole			Diastole			Time-averaged		
	Baseline (95% CI)	5 years (95% CI)	*P*-value	Baseline (95% CI)	5 years (95% CI)	*P*-value	Baseline (95% CI)	5 years (95% CI)	*P*-value
Maximum viscosity	8.84 ± 1.79 (4.01 to 13.70)	5.33 ± 3.63 (-5.31 to 13.25)	0.043	4.46 ± 1.50 (0.23 to 7.88)	3.18 ± 0.90 (0.58 to 5.52)	0.063	4.30 ± 1.54 (-0.08 to 7.82)	3.21 ± 0.57 (1.51 to 4.84)	0.028

Relative viscosity is expressed as a ratio of non-Newtonian viscosity to the constant Newtonian viscosity (0.0035 Pa s). Maximum viscosity values are presented as relative viscosity ± standard deviation.
CI, confidence interval; Pa, pascal.

First, higher ESS values immediately after scaffold implantation are significantly correlated with lumen enlargement by 5 years. Several intravascular ultrasound based studies in native arteries and OCT-based studies in scaffolded arteries suggest a similar relationship between ESS and subsequent vessel change.[36,39–42] Whether this phenomenon is unique to polymeric bioresorbable devices is unknown, but the consistent upward shift in ESS values observed in this study may continue to push the balance toward positive Glagovian remodelling and late lumen enlargement.[8,43–45]

Second, there is significant fluctuation in ESS and relative blood viscosity throughout the cardiac cycle, indicating that coronary arteries experience extreme absolute values and sudden shifts in local haemodynamics with each heartbeat. Exceptionally high ESS values identified in diastole are notable given the putative role of high ESS in platelet activation, plaque destabilisation, and perhaps even rupture.[33,35,46] Conversely, the rapid drop in coronary flow at the onset of systole unmasks micro-recirculation of blood between scaffold struts, reflecting areas prone to momentary blood stagnation and high viscosity in every cardiac cycle. In fact, after scaffold implantation blood manifested up to a 10-fold increase in relative viscosity around scaffold struts during systole. Some regions of high viscosity persisted even in diastole.

Third, regardless of time point within the cardiac cycle, all cases demonstrated homogenisation of ESS over 5 years, with less exposure to atherogenic low ESS and increased exposure to moderate and high ESS which are generally thought to be more atheroprotective. Critically, this was accompanied by a significant reduction in maximum blood viscosity. Immediately after implantation, micro-recirculation, low ESS, and high peak viscosity within the scaffolded region may contribute to early accumulation of fibrin, platelets, and other blood components just distal to each strut.[47] In a sense, the scaffold may act as a template for neointimal growth between struts as these aggregated materials organize. Once neointimal tissue has grown to cover the struts and the lumen surface becomes smooth, the alternans of high and low ESS dissipates, overall ESS increases, and peak viscosity is reduced. In such an ideal scenario there is no longer strong stimulus for thrombosis or neointimal hyperplasia. Remarkably, as bioresorbable devices dissolve, underlying arteries have demonstrated a partial and gradual return of normal arterial vasoreactivity and plaque stabilisation in addition to late lumen gain.[4–7] We postulate that some of these observations may be related to the normalisation of haemodynamics after scaffold implantation.

Although none of the patients in the current study developed adverse clinical events during 5 years of follow-up, our findings may add to previous work in explaining certain mechanisms of scaffold thrombosis and the potential mechanisms of long-term benefit. Factors associated with very late scaffold thrombosis include poor neointimal healing, uncovered struts, and persistent scaffold malapposition.[32] In some cases, suboptimal local haemodynamics immediately after scaffold implantation may contribute to poor neointimal growth and persistently uncovered or malapposed struts.[17] Such struts protruding into the lumen are exposed to high ESS, which is associated with platelet activation.[46] Regions distal to protruding struts are prone to low ESS and high viscosity, where activated platelets can aggregate.

Non-Newtonian simulations provide uniquely complementary haemodynamic data about blood viscosity. Blood is a non-Newtonian fluid with primarily shear-thinning properties: at low shear rates blood is thick, but at high shear rates it becomes thinner with viscosity approaching a constant. Although most arterial CFD simulations safely assume that blood behaves as a Newtonian fluid with a constant viscosity, under certain flow conditions the local shear rate can drop enough that the Newtonian assumption no longer holds.[48–51] This appears to be the case in coronary arteries under pulsatile flow and harbouring curvatures and scaffolds: even after averaging viscosity throughout each entire simulated artery, relative blood viscosity was approximately 35% greater than the Newtonian model, a finding consistent with previous studies in unstented arteries.[29,52–54] That we have demonstrated discrete and consistent increases in blood viscosity in patient-specific scaffolded coronary arteries suggests that the Newtonian assumption may not always be accurate in this setting.

The ability to measure local blood viscosity in vivo has the potential to add an entirely new dimension to the study of local arterial haemodynamics. Although some clinical evidence points to a correlation between higher plasma viscosity and coronary disease,[55] whether and how local blood viscosity relates to clinical outcomes will require much larger dedicated studies. Additionally, previous CFD studies suggest that neglecting non-Newtonian behaviours of blood may reduce the accuracy of ESS measurements.[48–50] This may partially explain the persistent limitation of ESS to detect and predict progressive atherosclerosis.[56] It is possible that in combination with traditional wall-based haemodynamic metrics, non-Newtonian simulations and viscosity calculations may improve the accuracy and specificity of CFD simulations by identifying areas at risk for platelet

activation, blood stagnation, plaque growth, neointimal hyperplasia, and thrombosis.

Limitations

This study has several limitations that must be acknowledged. First is the retrospective design, which means that OCT acquisition techniques to optimise arterial reconstruction were not specified in the original protocol. Second is the low number of cases studied. This was related to the low number of patients with serial OCT in the original study, but also to the absence of pre-defined OCT acquisition standards leading to several OCT studies that were suboptimal for arterial reconstruction. Due to our strict exclusion criteria, all such cases were excluded from CFD analysis, contributing to the low number of cases. Despite a small sample size, the overall consistency of our results suggests that the observations may indeed merit further investigation through dedicated pre-specified substudies of larger clinical device trials. Third, our analysis only included interval changes in lumen dimensions—it did not explicitly evaluate tissue characteristics. Quantitative OCT tissue characterisation is currently in development, and will provide further insights into the relationship between local haemodynamics and tissue changes in the future.[57] Fourth, although differences in scaffold architecture, connector design, and strut geometry will alter the haemodynamic microenvironment, CFD principles are universal and remain operational in the analysis of other scaffold designs.[58] Using CFD, our group has investigated two other scaffold designs with different strut thicknesses, the Mirage Bioresorbable Microfiber Scaffold (125 μm) and the ArterioSorb scaffold (95 μm). In both preclinical and randomized clinical trials, we have demonstrated that the circular struts of the Mirage become better embedded such that the area of laminar flow disturbances and low ESS were reduced from 49.30% in Absorb to 24.48% in Mirage ($P < 0.0001$).[59–61] In addition, using pulsatile and non-Newtonian CFD, we have shown that the ArterioSorb scaffold exhibits major reductions in area of low ESS area compared to Absorb, and in fact shear stress assessment has been reported as 'a method to differentiate bioresorbable scaffold platforms'.[58]

Conclusion

In conclusion, high fidelity pulsatile non-Newtonian CFD simulations reveal micro- and macro-level haemodynamics in scaffolded coronary arteries. Early haemodynamic disturbances induced after scaffold implantation may direct subsequent neointimal growth as the scaffold degrades, leading to more physiological ESS, reduced peak blood viscosity, and in some cases lumen enlargement. The ability to identify intravascular regions of high blood viscosity may have implications for further clinical characterisation of thrombosis, neointimal growth, and vessel healing.

Supplementary material

Supplementary material is available at *European Heart Journal* online.

Funding

This work has been partially supported by the Victorian Life Sciences Computation Initiative (VLSCI grant number VR0210) on its Peak Computing Facility at the University of Melbourne, an initiative of the Victorian Government, Australia; the Australian Research Council through ARC Linkage Project LP120100233; and Abbott Vascular. TUBITAK (The Scientific Council of Turkey to E.T.).

Conflict of interest: P.W.S. and Y.O. are members of the International Advisory Board of Abbott Vascular. All other authors declare no competing interests.

References

1. Carrel A. *Suture of Blood Vessels and Transplantation of Organs*. Amsterdam: Elsevier; 1912.
2. Ellis SG, Kereiakes DJ, Metzger DC, Caputo RP, Rizik DG, Teirstein PS, Litt MR, Kini A, Kabour A, Marx SO, Popma JJ, McGreevy R, Zhang Z, Simonton C, Stone GW; ABSORB II Investigators. Everolimus-eluting bioresorbable scaffolds for coronary artery disease. *N Engl J Med* 2015;**373**:1905–1915.
3. Serruys PW, Ormiston J, van Geuns RJ, de Bruyne B, Dudek D, Christiansen E, Chevalier B, Smits P, McClean D, Koolen J, Windecker S, Whitbourn R, Meredith I, Wasungu L, Ediebah D, Veldhof S, Onuma Y. A polylactide bioresorbable scaffold eluting everolimus for treatment of coronary stenosis: 5-year follow-up. *J Am Coll Cardiol* 2016;**67**:766–776.
4. Brugaletta S, Heo JH, Garcia-Garcia HM, Farooq V, van Geuns RJ, de Bruyne B, Dudek D, Smits PC, Koolen J, McClean D, Dorange C, Veldhof S, Rapoza R, Onuma Y, Bruining N, Ormiston JA, Serruys PW. Endothelial-dependent vasomotion in a coronary segment treated by ABSORB everolimus-eluting bioresorbable vascular scaffold system is related to plaque composition at the time of bioresorption of the polymer: indirect finding of vascular reparative therapy? *Eur Heart J* 2012;**33**:1325–1333.
5. Brugaletta S, Radu MD, Garcia-Garcia HM, Heo JH, Farooq V, Girasis C, van Geuns RJ, Thuesen L, McClean D, Chevalier B, Windecker S, Koolen J, Rapoza R, Miquel-Hebert K, Ormiston J, Serruys PW. Circumferential evaluation of the neointima by optical coherence tomography after ABSORB bioresorbable vascular scaffold implantation: can the scaffold cap the plaque? *Atherosclerosis* 2012; **221**:106–112.
6. Gomez-Lara J, Brugaletta S, Farooq V, van Geuns RJ, De Bruyne B, Windecker S, McClean D, Thuesen L, Dudek D, Koolen J, Whitbourn R, Smits PC, Chevalier B, Morel MA, Dorange C, Veldhof S, Rapoza R, Garcia-Garcia HM, Ormiston JA, Serruys PW. Angiographic geometric changes of the lumen arterial wall after bioresorbable vascular scaffolds and metallic platform stents at 1-year follow-up. *JACC Cardiovasc Interv* 2011;**4**:789–799.
7. Lane JP, Perkins LE, Sheehy AJ, Pacheco EJ, Frie MP, Lambert BJ, Rapoza RJ, Virmani R. Lumen gain and restoration of pulsatility after implantation of a bioresorbable vascular scaffold in porcine coronary arteries. *JACC Cardiovasc Interv* 2014;**7**:688–695.
8. Otsuka F, Pacheco E, Perkins LE, Lane JP, Wang Q, Kamberi M, Frie M, Wang J, Sakakura K, Yahagi K, Ladich E, Rapoza RJ, Kolodgie FD, Virmani R. Long-term safety of an everolimus-eluting bioresorbable vascular scaffold and the cobalt-chromium XIENCE V stent in a porcine coronary artery model. *Circ Cardiovasc Interv* 2014;**7**:330–342.
9. Cassese S, Byrne RA, Ndrepepa G, Kufner S, Wiebe J, Repp J, Schunkert H, Fusaro M, Kimura T, Kastrati A. Everolimus-eluting bioresorbable vascular scaffolds versus everolimus-eluting metallic stents: a meta-analysis of randomised controlled trials. *Lancet* 2016;**387**:537–544.
10. Serruys PW, Chevalier B, Sotomi Y, Cequier A, Carrié D, Piek JJ, Van Boven AJ, Dominici M, Dudek D, McClean D, Helqvist S, Haude M, Reith S, de Sousa Almeida M, Campo G, Iñiguez A, Sabaté M, Windecker S, Onuma Y. Comparison of an everolimus-eluting bioresorbable scaffold with an everolimus-eluting metallic stent for the treatment of coronary artery stenosis (ABSORB II): a 3 year, randomised, controlled, single-blind, multicentre clinical trial. *Lancet* 2016;**388**:2479–2491.
11. Wykrzykowska JJ, Kraak RP, Hofma SH, van der Schaaf RJ, Arkenbout EK, Aj IJ, Elias J, van Dongen IM, Tijssen RY, Koch KT, Baan J Jr, Vis MM, de Winter RJ, Piek JJ, Tijssen JG, Henriques JP; AIDA Investigators. Bioresorbable scaffolds versus metallic stents in routine PCI. *N Engl J Med* 2017;**376**:2319–2328.
12. Martorell J, Santoma P, Kolandaivelu K, Kolachalama VB, Melgar-Lesmes P, Molins JJ, Garcia L, Edelman ER, Balcells M. Extent of flow recirculation governs

expression of atherosclerotic and thrombotic biomarkers in arterial bifurcations. *Cardiovasc Res* 2014;**103**:37–46.
13. Nam D, Ni CW, Rezvan A, Suo J, Budzyn K, Llanos A, Harrison D, Giddens D, Jo H. Partial carotid ligation is a model of acutely induced disturbed flow, leading to rapid endothelial dysfunction and atherosclerosis. *Am J Physiol Heart Circ Physiol* 2009;**297**:H1535–H1543.
14. LaDisa JF Jr, Olson LE, Douglas HA, Warltier DC, Kersten JR, Pagel PS. Alterations in regional vascular geometry produced by theoretical stent implantation influence distributions of wall shear stress: analysis of a curved coronary artery using 3D computational fluid dynamics modeling. *Biomed Eng Online* 2006; **5**:40.
15. Wentzel JJ, Whelan DM, van der Giessen W, van Beusekom HMM, Andhyiswara I, Serruys PW, Slager CJ, Krams R. Coronary stent implantation changes 3-D vessel geometry and 3-D shear stress distribution. *J Biomechanics* 2000;**33**: 1287–1295.
16. Balossino R, Gervaso F, Migliavacca F, Dubini G. Effects of different stent designs on local hemodynamics in stented arteries. *J Biomechanics* 2008;**41**:1053–1061.
17. Foin N, Gutierrez-Chico JL, Nakatani S, Torii R, Bourantas CV, Sen S, Nijjer S, Petraco R, Kousera C, Ghione M, Onuma Y, Garcia-Garcia HM, Francis DP, Wong P, Di Mario C, Davies JE, Serruys PW. Incomplete stent apposition causes high shear flow disturbances and delay in neointimal coverage as a function of strut to wall detachment distance: implications for the management of incomplete stent apposition. *Circ Cardiovasc Interv* 2014;**7**:180–189.
18. Kolandaivelu K, Swaminathan R, Gibson WJ, Kolachalama VB, Nguyen-Ehrenreich KL, Giddings VL, Coleman L, Wong GK, Edelman ER. Stent thrombogenicity early in high-risk interventional settings is driven by stent design and deployment and protected by polymer-drug coatings. *Circulation* 2011;**123**: 1400–1409.
19. Poon EK, Barlis P, Moore S, Pan WH, Liu Y, Ye Y, Xue Y, Zhu SJ, Ooi AS. Numerical investigations of the haemodynamic changes associated with stent malapposition in an idealised coronary artery. *J Biomech* 2014;**47**:2843–2851.
20. Serruys PW, Onuma Y, Ormiston JA, de Bruyne B, Regar E, Dudek D, Thuesen L, Smits PC, Chevalier B, McClean D, Koolen J, Windecker S, Whitbourn R, Meredith I, Dorange C, Veldhof S, Miquel-Hebert K, Rapoza R, García-García HM. Evaluation of the second generation of a bioresorbable everolimus drug-eluting vascular scaffold for treatment of de novo coronary artery stenosis: six-month clinical and imaging outcomes. *Circulation* 2010;**122**:2301–2312.
21. Tearney GJ, Regar E, Akasaka T, Adriaenssens T, Barlis P, Bezerra HG, Bouma B, Bruining N, Cho J-M, Chowdhary S, Costa MA, de Silva R, Dijkstra J, Di Mario C, Dudeck D, Falk E, Feldman MD, Fitzgerald P, Garcia H, Gonzalo N, Granada JF, Guagliumi G, Holm NR, Honda Y, Ikeno F, Kawasaki M, Kochman J, Koltowski L, Kubo T, Kume T, Kyono H, Lam CCS, Lamouche G, Lee DP, Leon MB, Maehara A, Manfrini O, Mintz GS, Mizuno K, Morel M-A, Nadkarni S, Okura H, Otake H, Pietrasik A, Prati F, Räber L, Radu MD, Rieber J, Riga M, Rollins A, Rosenberg M, Sirbu V, Serruys PWJC, Shimada K, Shinke T, Shite J, Siegel E, Sonada S, Suter M, Takarada S, Tanaka A, Terashima M, Troels T, Uemura S, Ughi GJ, van Beusekom HMM, van der Steen AFW, van Es G-A, van Soest G, Virmani R, Waxman S, Weissman NJ, Weisz G; International Working Group for Intravascular Optical Coherence Tomography (IWG-IVOCT). Consensus standards for acquisition, measurement, and reporting of intravascular optical coherence tomography studies: a report from the International Working Group for Intravascular Optical Coherence Tomography Standardization and Validation. *J Am Coll Cardiol* 2012; **59**:1058–1072.
22. Bourantas CV, Papafaklis MI, Lakkas L, Sakellarios A, Onuma Y, Zhang YJ, Muramatsu T, Diletti R, Bizopoulos P, Kalatzis F, Naka KK, Fotiadis DI, Wang J, Garcia Garcia HM, Kimura T, Michalis LK, Serruys PW. Fusion of optical coherence tomographic and angiographic data for more accurate evaluation of the endothelial shear stress patterns and neointimal distribution after bioresorbable scaffold implantation: comparison with intravascular ultrasound-derived reconstructions. *Int J Cardiovasc Imaging* 2014;**30**:485–494.
23. Cignoni P, Callieri M, Corsini M, Dellepiane M, Ganovelli F, Ranzuglia G. MeshLab: an Open-Source Mesh Processing Tool. In: V Scarano, R De Chiara, U Erra, eds. *Sixth Eurographics Italian Chapter Conference*. Eurographics Association; 2008. p129–136.
24. Quemada D. Rheology of concentrated disperse systems II. A model for non-newtonian shear viscosity in steady flows. *Rheol Acta* 1978;**17**:632–642.
25. Dewey CFJ. Fluid mechanics of arterial flow. In: S Wolf, NT Werthessen, eds. *Advances in Experimental Medicine and Biology*. New York and London: Plenum; 1979. p55–103.
26. Levesque MJ, Sprague EA, Schwartz CJ, Nerem RM. Influence of shear stress on cultured vacsular endothelial cells: the stress response of an anchorage-dependent mammalian cell. *Biotechnol Progr* 1989;**5**:1–8.
27. Malek AM, Alper SL, Izumo S. Hemodynamic shear stress and its role in atherosclerosis. *JAMA* 1999;**282**:2035–2042.
28. Ballyk PD, Steinman DA, Ethier CR. Simulation of non-Newtonian blood flow in an end-to-end anastomosis. *Biorheology* 1994;**31**:565–586.
29. Johnston BM, Johnston PR, Corney S, Kilpatrick D. Non-Newtonian blood flow in human right coronary arteries: steady state simulations. *J Biomech* 2004;**37**: 709–720.
30. CLSI. Defining, establishing, and verifying reference intervals in the clinical laboratory: approved guideline – 3rd ed. CLSI Document C28–A3. Wayne, PA: Clinical and Laboratory Standards Institute; 2008.
31. Collet C, Asano T, Miyazaki Y, Tenekecioglu E, Katagiri Y, Sotomi Y, Cavalcante R, de Winter RJ, Kimura T, Gao R, Puricel S, Cook S, Capodanno D, Onuma Y, Serruys PW. Late thrombotic events after bioresorbable scaffold implantation: a systematic review and meta-analysis of randomized clinical trials. *Eur Heart J* 2017;**38**:2559–2566.
32. Raber L, Brugaletta S, Yamaji K, O'Sullivan CJ, Otsuki S, Koppara T, Taniwaki M, Onuma Y, Freixa X, Eberli FR, Serruys PW, Joner M, Sabate M, Windecker S. Very late scaffold thrombosis: intracoronary imaging and histopathological and spectroscopic findings. *J Am Coll Cardiol* 2015;**66**:1901–1914.
33. Bark DL Jr, Ku DN. Wall shear over high degree stenoses pertinent to atherothrombosis. *J Biomechanics* 2010;**43**:2970–2977.
34. Bark DL, Para AN, Ku DN. Correlation of thrombosis growth rate to pathological wall shear rate during platelet accumulation. *Biotechnol Bioeng* 2012;**109**: 2642–2650.
35. Fukumoto Y, Hiro T, Fujii T, Hashimoto G, Fujimura T, Yamada J, Okamura T, Matsuzaki M. Localized elevation of shear stress is related to coronary plaque rupture: a 3-dimensional intravascular ultrasound study with in-vivo color mapping of shear stress distribution. *J Am Coll Cardiol* 2008;**51**:645–650.
36. Stone PH, Coskun AU, Kinlay S, Popma JJ, Sonka M, Wahle A, Yeghiazarians Y, Maynard C, Kuntz RE, Feldman CL. Regions of low endothelial shear stress are the sites where coronary plaque progresses and vascular remodelling occurs in humans: an in vivo serial study. *Eur Heart J* 2007;**28**:705–710.
37. Foin N, Torii R, Mattesini A, Wong P, Di Mario C. Biodegradable vascular scaffold: is optimal expansion the key to minimising flow disturbances and risk of adverse events? *EuroIntervention* 2015;**10**:1139–1142.
38. Bourantas CV, Raber L, Zaugg S, Sakellarios A, Taniwaki M, Heg D, Moschovitis A, Radu M, Papafaklis MI, Kalatzis F, Naka KK, Fotiadis DI, Michalis LK, Serruys PW, Garcia Garcia HM, Windecker S. Impact of local endothelial shear stress on neointima and plaque following stent implantation in patients with ST-elevation myocardial infarction: a subgroup-analysis of the COMFORTABLE AMI-IBIS 4 trial. *Int J Cardiol* 2015;**186**:178–185.
39. Corban MT, Eshtehardi P, Suo J, McDaniel MC, Timmins LH, Rassoul-Arzrumly E, Maynard C, Mekonnen G, King S 3rd, Quyyumi AA, Giddens DP, Samady H. Combination of plaque burden, wall shear stress, and plaque phenotype has incremental value for prediction of coronary atherosclerotic plaque progression and vulnerability. *Atherosclerosis* 2014;**232**:271–276.
40. Bourantas CV, Papafaklis MI, Kotsia A, Farooq V, Muramatsu T, Gomez-Lara J, Zhang YJ, Iqbal J, Kalatzis FG, Naka KK, Fotiadis DI, Dorange C, Wang J, Rapoza R, Garcia-Garcia HM, Onuma Y, Michalis LK, Serruys PW. Effect of the endothelial shear stress patterns on neointimal proliferation following drug-eluting bioresorbable vascular scaffold implantation: an optical coherence tomography study. *JACC Cardiovasc Interv* 2014;**7**:315–324.
41. Eshtehardi P, McDaniel MC, Suo J, Dhawan SS, Timmins LH, Binongo JN, Golub LJ, Corban MT, Finn AV, Oshinski JN, Quyyumi AA, Giddens DP, Samady H. Association of coronary wall shear stress with atherosclerotic plaque burden, composition, and distribution in patients with coronary artery disease. *J Am Heart Assoc* 2012;**1**:e002543.
42. Samady H, Eshtehardi P, McDaniel MC, Suo J, Dhawan SS, Maynard C, Timmins LH, Quyyumi AA, Giddens DP. Coronary artery wall shear stress is associated with progression and transformation of atherosclerotic plaque and arterial remodeling in patients with coronary artery disease. *Circulation* 2011;**124**: 779–788.
43. Glagov S, Weisenberg E, Zarins CK, Stankunavicius R, Kolettis G. Compensatory enlargement of human atherosclerotic coronary arteries. *N Engl J Med* 1987;**316**: 1371–1375.
44. Zarins CK, Zatina MA, Giddens DP, Ku DN, Glagov S. Shear stress regulation of artery lumen diameter in experimental atherogenesis. *J Vasc Surg* 1987;**5**: 413–420.
45. Onuma Y, Collet C, van Geuns RJ, de Bruyne B, Christiansen E, Koolen J, Smits P, Chevalier B, McClean D, Dudek D, Windecker S, Meredith I, Nieman K, Veldhof S, Ormiston J, Serruys PW; ABSORB Investigators. Long-term serial non-invasive multislice computed tomography angiography with functional evaluation after coronary implantation of a bioresorbable everolimus-eluting scaffold: the ABSORB cohort B MSCT substudy. *Eur Heart J Cardiovasc Imaging* 2017;**18**:870–879.

46. Holme PA, Orvim U, Hamers MJAG, Solum NO, Brosstad FR, Barstad RM, Sakariassen KS. Shear-induced platelet activation and platelet microparticle formation at blood flow conditions as in arteries with a severe stenosis. *Arterioscler Thromb Vasc Biol* 1997;**17**:646–653.
47. Jimenez JM, Prasad V, Yu MD, Kampmeyer CP, Kaakour AH, Wang PJ, Maloney SF, Wright N, Johnston I, Jiang YZ, Davies PF. Macro- and microscale variables regulate stent haemodynamics, fibrin deposition and thrombomodulin expression. *J R Soc Interface* 2014;**11**:20131079.
48. Karimi S, Dabagh M, Vasava P, Dadvar M, Dabir B, Jalali P. Effect of rheological models on the hemodynamics within human aorta: CFD study on CT image-based geometry. *J Nonwewton Fluid Mech* 2014;**207**:42–52.
49. van Wyk S, Prahl Wittberg L, Bulusu KV, Fuchs L, Plesniak MW. Non-Newtonian perspectives on pulsatile blood-analog flows in a 180° curved artery model. *Phys Fluids* 2015;**27**:071901.
50. van Wyk S, Prahl Wittberg L, Fuchs L. Wall shear stress variations and unsteadiness of pulsatile blood-like flows in 90-degree bifurcations. *Comput Biol Med* 2013;**43**:1025–1036.
51. Gijsen FJH, van de Vosse FN, Janssen JD. The influence of the non-Newtonian properties of blood on the flow in large arteries: steady flow in a carotid bifurcation model. *J Biomech* 1999;**32**:601–608.
52. Soulis JV, Giannoglou GD, Chatzizisis YS, Seralidou KV, Parcharidis GE, Louridas GE. Non-Newtonian models for molecular viscosity and wall shear stress in a 3D reconstructed human left coronary artery. *Med Eng Phys* 2008;**30**:9–19.
53. Johnston BM, Johnston PR, Corney S, Kilpatrick D. Non-Newtonian blood flow in human right coronary arteries: transient simulations. *J Biomech* 2006;**39**:1116–1128.
54. Soulis JV, Farmakis TM, Giannoglou GD, Hatzizisis IS, Giannakoulas GA, Parcharidis GE, Louridas GE. Molecular viscosity in the normal left coronary arterial tree. Is it related to atherosclerosis? *Angiology* 2006;**57**:33–40.
55. Junker R, Heinrich J, Ulbrich H, Schulte H, Schonfeld R, Kohler E, Assmann G. Relationship between plasma viscosity and the severity of coronary heart disease. *Arterioscler Thromb Vasc Biol* 1998;**18**:870–875.
56. Peiffer V, Sherwin SJ, Weinberg PD. Does low and oscillatory wall shear stress correlate spatially with early atherosclerosis? A systematic review. *Cardiovasc Res* 2013;**99**:242–250.
57. Liu S, Sotomi Y, Eggermont J, Nakazawa G, Torii S, Ijichi T, Onuma Y, Serruys PW, Lelieveldt BPF, Dijkstra J. Tissue characterization with depth-resolved attenuation coefficient and backscatter term in intravascular optical coherence tomography images. *J Biomed Opt* 2017;**22**:1–16.
58. Tenekecioglu E, Torii R, Bourantas CV, Al-Lamee R, Serruys PW. Non-Newtonian pulsatile shear stress assessment: a method to differentiate bioresorbable scaffold platforms. *Eur Heart J* 2017;**38**:2570.
59. Tenekecioglu E, Torii R, Sotomi Y, Collet C, Dijkstra J, Miyazaki Y, Crake T, Su S, Costa R, Chamie D, Liew HB, Santoso T, Onuma Y, Abizaid A, Bourantas CV, Serruys PW. The effect of strut protrusion on shear stress distribution: hemodynamic insights from a prospective clinical trial. *JACC Cardiovasc Interv* 2017;**10**:1803–1805.
60. Tenekecioglu E, Serruys PW, Onuma Y, Costa R, Chamie D, Sotomi Y, Yu TB, Abizaid A, Liew HB, Santoso T. Randomized comparison of absorb bioresorbable vascular scaffold and mirage microfiber sirolimus-eluting scaffold using multimodality imaging. *JACC Cardiovasc Interv* 2017;**10**:1115–1130.
61. Tenekecioglu E, Torii R, Bourantas C, Sotomi Y, Cavalcante R, Zeng Y, Collet C, Crake T, Suwannasom P, Onuma Y, Serruys PW. Difference in hemodynamic microenvironment in vessels scaffolded with absorb BVS and mirage BRMS: insights from a pre-clinical endothelial shear stress study. *EuroIntervention* 2017;**13**:1327–1335.